

# Material-Specific User Colour Profiles from Imaging Spectroscopy Data

Lin Gu<sup>2</sup> Cong Phuoc Huynh<sup>1</sup> Antonio Robles-Kelly<sup>1,2</sup> Jun Zhou<sup>2\*</sup>

<sup>1</sup>NICTA, <sup>†</sup>Locked Bag 8001, Canberra ACT 2601, Australia

<sup>2</sup>School of Engineering, Australian National University, Canberra ACT 0200, Australia

## Abstract

*In this paper, we present a method which permits the creation of user colour preferences for object materials and lights in the scene making use of imaging spectroscopy data. To do this, we build upon the heterogeneous nature of the scene by imposing consistency over object materials so as to allow for small compositional variations across objects in the image. Once the consistency has been imposed, we aim at maximising the quality of the images under consideration based upon user input. This provides the flexibility necessary to utilise user profiles for the automatic processing of real world imagery while avoiding undesirable effects encountered when colour images are produced. We provide results on real-world imagery and illustrate how the method can be used to produce material-specific colours based upon user input.*

## 1. Introduction

In computer vision, video and graphics, we rely upon cameras and rendering contexts to capture and reproduce colour information. The accurate capture and reproduction of colours as acquired by digital cameras is an active area of research which has applications in colour correction [5, 11, 13, 27], camera simulation [20] and sensor design [10].

The quantification and measurement of the accuracy of the colours acquired by the camera with respect to human perception has evolved in a vast amount of literature on colorimetry and colour science [28]. In contrast with colorimetry, spectroscopy has as object of study the spectrum of light absorbed, transmitted, reflected or emitted by objects and illuminants in the scene. Multispectral and hyperspectral sensing devices can acquire wavelength-indexed reflectance and radiance data in tens or hundreds of bands across a broad spectral range. Thus, multi-spectral and hyperspectral image sensors can provide an information-rich



Figure 1. Left-hand panel: Pseudocolour hyperspectral image; Right-hand panel: Image resulting from editing the rose color.

representation of the spectral response of materials [7].

The material spectral reflectance together with illuminant power spectrum measurements, can be used to perform colorimetric simulation [26]. This is often based upon the assumption that the RGB values in the image are linear combinations of the device-independent CIE colour matching functions [6]. In this paper, we consider the case where scene colours are reproduced based upon particular materials and lights. That is, rather than computing the RGB values using the standard colour matching functions [25], we aim at producing colour associated with materials and illuminants in the scene. An example of image editing with respect to materials in the scene is shown in Figure 1. In the figure, we assigned a purple hue to the rose as an alternative to the red in the input image. As a result, the rose turns purple while the red pot in the scene remains unaffected.

Here, we present a method for the creation of user color preferences based upon the materials in the scene from imaging spectroscopy data. The main advantage of the approach presented here stems from the fact that imaging spectroscopy is robust to metamerism. Recall that, traditionally, colour editing [3], image equalisation [29] and colour transfer [12] approaches based on RGB suffer from the drawbacks introduced by the possibility of having two materials with the same colour but dissimilar reflectance. The formulation presented here can allow complex photowork [18] in which images are edited, modified, annotated, *etc.* based upon object materials, illuminants and user preferences rather than RGB values.

\*The work presented here was done while Jun Zhou was with NICTA.

<sup>†</sup>NICTA is funded by the Australian Government as represented by the Department of Broadband, Communications and the Digital Economy and the Australian Research Council through the ICT Centre of Excellence program.

## 2. Background

We tackle the following problem. Let us consider a multispectral or hyperspectral image with the spatial domain  $\mathcal{I}$  consisting of wavelength-indexed radiance spectra in the visible spectrum. The aim of computation becomes the recovery of a colour image which corresponds to the input imagery where the RGB colour of the materials in the scene is determined by user input. This is done using two libraries. The first of these is given by the set  $\mathbf{S}$  of primordial materials or end members which account for object materials in the scene. These end members can be any man-made or natural materials such as plastic, metals, skin, *etc.* The second library corresponds to “canonical” illuminant power spectra corresponding to light sources which commonly occur in real world environments. Similarly to our end members above, these are lights that can be viewed as widespread in natural and man-made environments, such as sunlight, neon tubes, tungsten lighting, *etc.*

To each of our end members or canonical light sources corresponds a colour mapping function that yields a tristimulus RGB value for each of the entries in the libraries. To recover the colour mappings and provide a means to their computation we adopt the dichromatic model introduced by Shafer [24]. The model decomposes the scene radiance  $I(\lambda, v)$  at pixel  $v$  and wavelength  $\lambda$  into a diffuse and a specular component as follows

$$I(\lambda, v) = L(\lambda)(g(v)S(\lambda, v) + k(v)) \quad (1)$$

where  $L(\cdot)$  is the illuminant power spectrum,  $S(\lambda, v)$  is the object reflectance, the shading factor  $g(v)$  governs the proportion of diffuse light reflected from the object and the factor  $k(v)$  models surface irregularities that cause specularities in the scene.

Once an image is acquired, the dichromatic parameters are computed using the algorithm in [15]. The regions in the image corresponding to objects sharing the same material reflectance are recovered so as to select end members in the library with the closest affinity. This process prevents break-up of objects which, despite being made of the same material, present small variations in reflectance found in real-world materials. Here, we build upon the aesthetic rating method in [8] so as to recover the colour preferences for the materials and illuminants in the libraries, which maximises both their accordance with the user input and the ratings of the imagery that the user is editing. In this way, changes in the end-member colour mappings will be “moderated” by the aesthetic scores.

Following colorimetry theory [28] and by noting that the image formation process applies equally to each of the three colour channels, we can use the index  $c = \{R, G, B\}$  so as to write the RGB values for the colour image as follows

$$I_c(v) = \kappa_c \int_V H_c(\lambda) I(\lambda, v) d\lambda \quad (2)$$

where  $V$  is the human visible spectrum, *i.e.*  $\lambda \in [390nm, 750nm]$  and  $H_c(\lambda)$  is the value of the colour matching function [25] for channel  $c$  at the wavelength  $\lambda$ . The value of  $\kappa_c$  in Equation 2 corresponds to the colour balance factor of the camera against a predetermined reference.

As mentioned earlier, we aim at providing a means to computing material-specific colours. To this end, we express the image radiance using the mixture coefficient  $\rho_{m,v}$  of the material  $m$  in the composition of the pixel  $v$  and the mixture coefficient  $\alpha_\ell$  of the canonical illuminant  $\ell$ , as follows

$$I_c(v) = \left( \sum_{\ell=1}^M \alpha_\ell g_\ell(\mathbf{L}_\ell(\cdot)) \right) \left( g(v) \sum_{m=1}^N \rho_{m,v} f_c(\mathbf{S}_m(\cdot)) + k(v) \right) \quad (3)$$

where  $\mathbf{S}_m(\cdot)$  is the vectorial representation of the reflectance spectrum of the end-member with the indexed  $m$  in the material library  $\mathbf{S}$ ,  $\mathbf{L}_\ell$  is the power spectrum of the  $\ell^{th}$  entry in our library of  $M$  canonical illuminants and  $g_\ell(\cdot)$  and  $f_c(\cdot)$  are the colour mapping functions that assign a tristimulus to each combination of canonical illuminant power and end member reflectance.

Since the values yielded by these functions are dependent on the illuminants and materials in the scene, the colours in the image can be computed with respect to the light and object matter rather than an integration of the spectral values subject to the colour matching function. We would like to stress that such decompositions have been used elsewhere [9, 17, 22]. Our main contribution pertains to a method by which material consistency can be imposed and the user input can be used for the computation of the mixture coefficients  $\rho_{m,v}$  and  $\alpha_\ell$  so as to recover an RGB image corresponding to the input hyperspectral imagery.

It is worth noting that this is somewhat related to interactive recolouring approaches [1, 21]. It is also somewhat related to the idea of applying user preferences to one-to-one colour transfer operations between images [23]. The work presented here, however, differs from these in a number of ways. In our approach, we employ imaging spectroscopy to recover the photometric parameters and reflectance, recovering the profiles making use of an optimisation process which takes into account the aesthetics of the images in a reference data set. In Figure 2 we show a diagrammatic realisation of the method. This has two stages, which pertain to both the way in which the user profile is generated and the colour imagery is produced. Note that, for the generation of the profiles, an image data set is used to train a classifier. This classifier is then used to recover the aesthetics scores used for the recovery of the colour matching functions of the user preference. Subsequently, these matching functions are used to generate user-preferred colour values corresponding to novel input images. For both cases, the system has an built-in library of canonical illuminants and

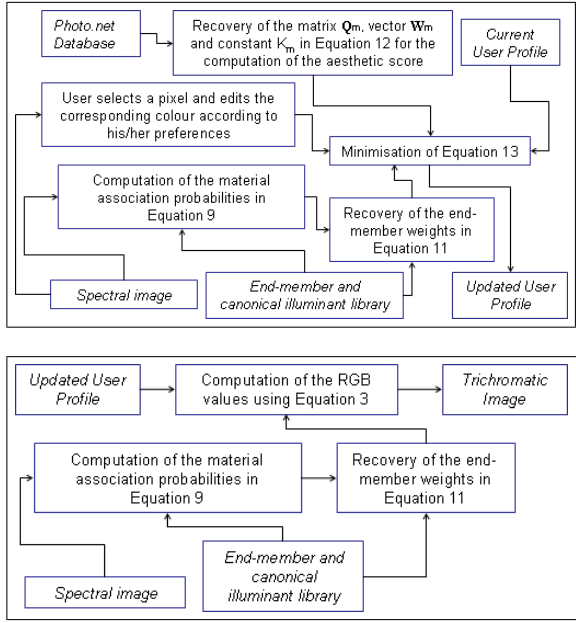


Figure 2. Top panel: Diagram for the recovery of the colour matching functions for the user profile; Bottom panel: Diagram for the generation of colour imagery from the user profiles.

end-members. In the following sections, we elaborate further on each of the steps in Figure 2.

### 3. Colour Profiles from User Input

As mentioned earlier, to recover colour imagery dependent on user-defined preferences, we build upon the heterogeneous nature of the scene by imposing consistency over object materials. Once consistency has been imposed, we aim at maximising the aesthetic quality of the images under consideration. In this section, we present both our consistency imposition approach and a method upon which the aesthetic scores of the imagery are used to moderate the changes in the mixture coefficients  $\rho_{m,v}$ .

#### 3.1. Imposing End-member Consistency

Note that, in practice, there may be variations in the actual reflectance of pixels belonging to the same material in the scene. This does not necessarily indicate a change of the object material under consideration rather than small variations in composition. For instance, the spatial variations on the enamel of a mug entirely made of porcelain may result in changes in the end-member association to each pixel and adversely affect the colour finally produced. Hence, it would be rather undesirable to have objects partitioned or fragmented into inconsistent end-members as the colour image is produced.

In this section, we aim at imposing end member consistency between pixels sharing the same material in the

scene using the reflectance spectra obtained by the algorithm in [15]. Instead of solving the problem at the pixel level, we extend the problem to material clusters, where the end member decomposition occurs per material rather than per pixel.

##### 3.1.1 Cost Function

We impose consistency of end-member composition by recovering their mixture coefficients for each material from the mean reflectance spectrum of the material. To this end, we assign a partial membership  $P(\omega|v)$  of a material cluster  $\omega$  with mean reflectance  $\mathbf{S}_\omega(\cdot)$  to each pixel  $v$  in the image. Taking the set of all the material clusters  $\Omega$  in the scene into account, we view the recovery of the mixture coefficients as two successive optimisation problems. The first of these considers the clustering of image pixels based on their spectral reflectance. Here, we employ an affinity metric  $a(\omega, v)$  to preselect  $k$  end members per material. This is done using the affinity between the pixel reflectance spectrum  $\mathbf{S}(\cdot, v)$  and the mean spectrum  $\mathbf{S}_\omega(\cdot)$  of a material cluster. Mathematically, this affinity measure can be defined by their Euclidean angle

$$a(\omega, v) = 1 - \frac{\langle \mathbf{S}(\cdot, v), \mathbf{S}_\omega(\cdot) \rangle}{\|\mathbf{S}(\cdot, v)\| \|\mathbf{S}_\omega(\cdot)\|} \quad (4)$$

With this metric, the first optimisation problem aims to minimise the total expected affinity for the entire image as

$$A_{Total} = \sum_{v \in \mathcal{I}, \omega \in \Omega} P(\omega|v) a(\omega, v) \quad (5)$$

subject to the law of total probability  $\sum_{\omega \in \Omega} P(\omega|v) = 1 \forall v \in \mathcal{I}$ .

Since the formulation in Equation 5 often favours hard assignment of pixels to their closest materials, we restate the problem subject to the maximum entropy criterion [16]. The entropy of the material association probability distribution at each pixel is defined as

$$\mathcal{P} = - \sum_{v \in \mathcal{I}} \sum_{\omega \in \Omega} P(\omega|v) \log P(\omega|v) \quad (6)$$

With the affinity metric in Equation 4, the problem becomes that of finding a set of object material spectra and a distribution of material association probabilities  $P(\omega|v)$  for each pixel  $v$  so as to minimise  $A_{Entropy} = A_{Total} - \mathcal{L}$  where

$$\mathcal{L} = T\mathcal{P} + \sum_{v \in \mathcal{I}} \varrho(v) \left( \sum_{\omega \in \Omega} P(\omega|v) - 1 \right) \quad (7)$$

in which  $T \geq 0$  and  $\varrho(v)$  are Lagrange multipliers. Note that  $T$  weighs the level of randomness of the material association probabilities whereas  $\varrho(v)$  enforces the total probability constraint for every image pixel  $v$ .

The optimisation approach to the problem is somewhat similar to an annealing soft-clustering process. At the beginning, this process is initialised assuming all the image pixels are made of the same material. As the method progresses, the set  $\Omega$  of materials grows. This, in essence, constitutes several “phase transitions”, at which new materials arise from the existing ones. This phenomenon is due to the discrepancy in the affinity  $a(\omega, v)$  between the pixel reflectance  $\mathbf{S}(\cdot, v)$  and the material reflectance spectrum  $\mathbf{S}_\omega(\cdot)$ .

### 3.1.2 Material Reflectance and End-Member Proportion Recovery

We now derive the optimal set  $\Omega$  of scene materials so as to minimise the cost function above. To do this, we compute the derivatives of  $A_{Entropy}$  with respect to the material reflectance spectrum  $\omega(\cdot)$  and equate it to zero, which yields

$$\mathbf{S}_\omega(\cdot) \propto \sum_{v \in \mathcal{I}} P(\omega|v) \frac{\mathbf{S}(\cdot, v)}{\|\mathbf{S}(\cdot, v)\|} \quad (8)$$

In Equation 8, we require the probability  $P(\omega|v)$  to be available. To compute this probability, we employ deterministic annealing. A major advantage of the deterministic annealing approach is that it avoids being attracted to local minima. In addition, deterministic annealing converges faster than stochastic or simulated annealing [19].

The deterministic annealing approach casts the Lagrangian multiplier  $T$  as a system temperature. At each phase of the annealing process, where the temperature  $T$  is kept constant, the algorithm proceeds as two interleaved minimisation steps so as to arrive at an equilibrium state. These two minimisation steps are performed alternately with respect to the material association probabilities and the end members.

For the recovery of the pixel-to-material association probabilities, we fix the material reflectance spectrum  $\mathbf{S}_\omega(\cdot)$  and seek for the probability distribution which minimises the cost function  $A_{Entropy}$ . This is achieved by setting the partial derivative of  $A_{Entropy}$  with respect to  $P(\omega|v)$  to zero. Since  $\sum_{\omega \in \Omega} P(\omega|v) = 1$ , it can be shown that the optimal material association probability for a fixed material set  $\Omega$  is given by the Gibbs distribution

$$P(\omega|v) = \frac{\exp\left(\frac{-a(\omega, v)}{T}\right)}{\sum_{\omega' \in \Omega} \exp\left(\frac{-a(\omega', v)}{T}\right)} \forall \omega, v \quad (9)$$

### 3.1.3 Recovery of End-member Coefficients

Now, we pay attention to the problem concerned with the decomposition of the mean material reflectance spectra into end-member proportions. With the material reflectance

$\mathbf{S}_\omega(\cdot)$  in hand, we recover the end-member proportions  $\rho_{m, \omega}$  contributing to the composition of each material  $\omega$ . The problem is formulated as a minimisation of the cost function

$$\epsilon_\omega = \int_V \left( S_\omega(\lambda) - \sum_{m=1}^N \rho_{m, \omega} \mathbf{S}_m(\lambda) \right)^2 d\lambda \quad (10)$$

subject to the constraints  $\rho_{m, \omega} \geq 0$  and  $\sum_{m=1}^N \rho_{m, \omega} = 1 \forall \omega \in \Omega$ .

The cost function in Equation 10 can be minimised by a least-squares solver. The weight of the end-member  $m$  for pixel  $v$  is then given by

$$\rho_{m, v} = \sum_{\omega \in \Omega} P(\omega|v) \rho_{m, \omega} \quad (11)$$

## 3.2. Integration of Image Aesthetics

With the material clusters obtained, we proceed to the recovery of the user profile itself. Note that, in practice, the user can choose pixels in the image  $\mathcal{I}$  which he/she would like to edit and assign a color to their corresponding material. In this manner, the problem of recovering the relevant user profile becomes that of finding a strategy to update the function  $f_c(\cdot)$  for each end-member so as to recover the colours of the materials under consideration.

A straightforward solution here would be to solve a linear system of equations so as to recover the colour mapping functions based on, for instance, a least squares criterion. The main drawback of this treatment is that given a set of hyperspectral images, when the user edits the material in one of them, such an action will change the appearance of the other imagery. Thus, here we aim at moderating the effect of changes in the colour of library end-members for the material being edited. This is done using the aesthetic score of the rest of the imagery. The idea is to use the aesthetic qualities of some features in the images under study to recover the color mapping functions such that the material colour is as close as possible to that selected by the user on the image being edited while avoiding changes that would make the colour of the rest of the available images less aesthetically appealing.

### 3.2.1 The Aesthetic Score

To relate the update of the colour mapping functions to the aesthetic qualities of the imagery, we use eight features introduced in [8]. Note that, in [8], the authors classified images in terms of aesthetic quality by obtaining the top 15 out of 56 features which yield the highest classification accuracy. Following this approach, we used the eight features in their system which operate on HSV values. The reason for our choice stems from the fact that, being based upon the

Most abundant material	$\xi_{1,m} = \frac{\sum_{v \in \mathcal{I}} \rho_{m,v} \delta_{v,1}}{\sum_{v \in \mathcal{I}} \delta_{v,1}}$
2 <sup>nd</sup> -most abundant material	$\xi_{2,m} = \frac{\sum_{v \in \mathcal{I}} \rho_{m,v} \delta_{v,2}}{\sum_{v \in \mathcal{I}} \delta_{v,2}}$
Rule of Thirds	$\xi_{3,m} = \frac{h}{9} \sum_{v \in \mathcal{I}_{thirds}} \rho_{m,v}$
Whole image average	$\xi_{4,m} = h \sum_{v \in \mathcal{I}} \rho_{m,v}$
Macro Feature	$\xi_{5,m} = \frac{\sum_{v \in \mathcal{I}_{inner}} \rho_{m,v}}{\sum_{v \in \mathcal{I}_{rest}} \rho_{m,v}}$

Table 1. Aesthetic features per material in each image.

HSV values for the image, these features can be expressed in terms of our end-member library making use of a set of image-wise parameters which depend on the mixture coefficients  $\rho_{m,v}$ .

These features are computed as given by the formulae in Table 1. In the table, we present the parameters  $\xi_i$  computed making use of the mixture coefficients and the function  $\delta_{v,i}$ , which is unity if and only if the  $i^{th}$ -most abundant material in the image has a non-zero mixture coefficient in the composition of the pixel  $v$ . Making use of these features, we form the following feature vector to compute the aesthetic score  $\varphi_{\mathcal{I},m} = [\xi_{1,m}, \xi_{2,m}, \xi_{3,m}, \xi_{4,m}, \xi_{5,m}] \times \mathcal{S}_m, [\xi_{1,m}, \xi_{4,m}, \xi_{5,m}] \times \mathcal{V}_m]^T$  where  $\mathcal{S}_m$  and  $\mathcal{V}_m$  are the saturation and the brightness components of the HSV values equivalent to the RGB responses yielded by the colour mapping function  $f_c(\mathbf{S}_m(\cdot))$  for the end-member  $m$ . It is worth noting in passing that the omission of the hue component from the feature is not our choice but rather a direct development from [8] where hue does not appear in the top 15 features as a result of five-fold cross validation. This is somewhat desirable for our method since our optimisation approach will leave the hue to be edited by the user while allowing for variations of saturation and brightness.

We provide an interpretation of the above feature vector as follows. The features in Table 1, from top to bottom, correspond to the weighted average of the two most abundant materials in the image, the rule of thirds (the center square  $\mathcal{I}_{thirds}$  of the image when divided into a lattice of nine regions), the mean image-wise mixture coefficient and the macro weighted average per image. Here, following [8] we have computed the macro weighted average by dividing the image into a lattice of 16 regions so as to recover the four center squares denoted as  $\mathcal{I}_{inner}$  and the outer region denoted as  $\mathcal{I}_{rest}$  such that  $\mathcal{I} = \mathcal{I}_{inner} \cup \mathcal{I}_{rest}$ . In the table,  $h$  acts as a bandwidth parameter given by the quantity  $\frac{1}{|\mathcal{I}|}$ .

### 3.2.2 Color Mapping Update

To express the aesthetics of images in terms of the saturation, the brightness and the mixture coefficients of end-

members, we define the score  $\gamma_{\mathcal{I},m}$  for each image provided as input to the user. This score is computed making use of the set  $\Upsilon$  of images which will be affected in aesthetic terms by the colour mapping function update, although not being edited directly. Thus, the score of each end-member  $m$  in the image  $\mathcal{I}$  is given by the value of a quadratic discriminant as follows

$$\gamma_{\mathcal{I},m} = K_m + \varphi_{\mathcal{I},m}^T \mathbf{W}_m + \varphi_{\mathcal{I},m}^T \mathbf{Q}_m \varphi_{\mathcal{I},m} \quad (12)$$

where the matrix  $\mathbf{Q}_m$ , the vector  $\mathbf{W}_m$  and the constant  $K_m$  correspond to the end-member  $m$  in the library. These parameters can be recovered making use of quadratic discriminant analysis, which relaxes the constraint that both high and low aesthetic quality image groups have a common covariance structure, as compared to LDA.

Given the aesthetic score of the imagery, we now proceed to formulate the recovery of the colour mapping function for the end-members in an optimisation setting. Specifically, we aim to minimise the following cost function

$$\epsilon_{f_c} = \sum_{\mathcal{I} \in \Upsilon} \sum_{v \in \mathcal{I}} \left( I_c(v) - \sum_{m \in \mathbf{S}} \rho_{m,v} f_c(\mathbf{S}_m(\cdot)) \right)^2 + \tau \sum_{\mathcal{I} \in \Upsilon} \sum_{m \in \mathbf{S}} \exp(-\gamma_{\mathcal{I},m}) \quad (13)$$

In the above equation,  $I_c(v)$  is the value of the  $c$ -component at the pixel  $v$  as provided by the user while editing the image  $\mathcal{I}$ . To be consistent with the fact that the score  $\gamma_m$  is a quadratic function of the material HSV values  $\mathcal{S}_m$  and  $\mathcal{V}_m$ , we converted the user-provided pixel colour  $I_c(v)$  and the mapping  $f_c(\mathbf{S}_m(\cdot))$  to the HSV colour space. Furthermore,  $\tau$  is a parameter that controls the contribution of the aesthetic score  $\gamma_{\mathcal{I},m}$  in the optimisation process. Note that, in the equation above, we used the exponential as a monotonically decreasing function whose value tends to zero as the score of the imagery increases. This has the effect of penalising choices of  $f_c(\mathbf{S}_m(\cdot))$  which yield poor aesthetic results. In order to minimise the cost function in Equation 13, we employed a quasi-Newton method [4].

## 4. Implementation Issues

For the training of the quadratic discriminant model in Equation 12, we follow [8] and use the *Photo.net* database. This is an online photo sharing community where its members rate photos in the database from one to seven, while higher score indicates better aesthetic quality. For the recovery of the matrix  $\mathbf{Q}_m$ , the vector  $\mathbf{W}_m$  and the scalar  $K_m$ , we extracted features for the photos in the database and separate the images into high and low aesthetic quality. To do this, we use a cut-off rating of  $5.0 \pm \frac{t}{2}$  for the images of high and low aesthetic quality, where  $t$  is a parameter chosen by cross validation so as to maximise the accuracy of the quadratic estimator on the *Photo.net* database.

Also, note that one of the technical challenges in spectral image processing is the ability to compare and process spectral data acquired by heterogeneous sensing devices, which may vary in spectral resolution and range. For instance spectrometers are able to acquire hundreds of bands in the visible and infrared regions, whereas hyperspectral and multispectral imagers are often limited to a much coarser spectral resolution due to their optical design. In our implementation, the end-member library was collected with a spectrometer with a high spectral resolution, while the spectral imagery was acquired by a hyperspectral camera with a lower spectral resolution. To overcome this barrier, it is necessary to re-interpolate spectral data originally collected from these different sources so as to provide consistent spectral resolutions and ranges.

Furthermore, operations such as the object material recovery process in Section 3.1 do require spectra of equal lengths and resolutions. We have noted that there have been a number of representations of reflectance spectra using basis functions in the literature. These are, in essence, spectral descriptors which allow for the interpolation of spectral data by employing either a B-Spline [14] or a Gaussian Mixture representation [2]. In the experiments presented in Section 5, we employ the B-Spline representation to normalise the length and resolution of image and end-member spectra due to its superior performance to the Gaussian Mixture representation for material classification tasks [14].

We have designed a graphical user interface for users to provide their colour preferences. Initially, the image is rendered from the input spectral data using the colour matching functions in [25]. Subsequently, users select a pixel on the input image to change the colour of its material according to their preferences. Once a user finishes his/her edits, the system computes the dichromatic model parameters and the proportions of end-members as shown in Section 3.1 and updates the colour mapping functions as described in Section 3.2.2. Note that the application development hinges on the underlying assumption that each user has a particular colour profile. This is in general true, since trichromatic cameras fix the material-colour relationship making use of sensor-dependent colour matching functions. Thus, our application provides a means for the user to create and update a profile or profiles of his/her preferences.

Finally, to compute the colour mapping functions from user input, we require the user-provided colour at a number of image pixels. We note that, in Equation 3, the pixel colour is a linear combination of  $MN + M$  terms involving the functions  $f_c(\cdot)$  and  $g_c(\cdot)$ . Therefore, to recover the colour values  $C_m$ , we require at least  $MN + M$  pixel spectra to solve for the end-members and canonical light sources when the user edits the material colours. In practice, our interface employs a “dropper tool” which allows the user to edit the colour of a single pixel at a time. Therefore, the sys-

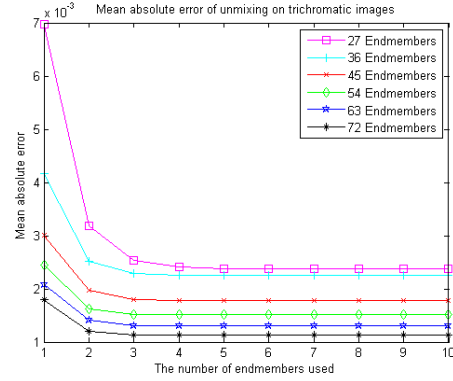


Figure 3. The mean absolute error of the pseudocolour imagery yielded by our method as compared to the colorimetric standard.

tem is designed to automatically select more pixels sharing the same material as that of the selected one using a similarity threshold. This similarity measure between two pixels  $u$  and  $v$  is reminiscent of that used in bilateral filtering, which is given by

$$d(u, v) = \exp \left\{ - \left( \frac{\angle(S(\cdot, u), S(\cdot, v))}{\sigma_r} \right)^2 - \left( \frac{\|u - v\|}{\sigma_s} \right)^2 \right\}$$

where  $\angle(S(\cdot, u), S(\cdot, v))$  is the Euclidean angle between the reflectance spectra,  $\|u - v\|$  is the spatial distance between  $u$  and  $v$ , and  $\sigma_r$  and  $\sigma_s$  signify the kernel widths in the spectral reflectance and spatial domains.

## 5. Experiments

In our experiments, the end-member library consists of 297 reflectance spectra acquired in house using a StellarNet spectrometer. The end-member spectra is sampled at a spectral resolution of  $1nm$  in the interval  $[430nm, 720nm]$ , *i.e.* the visible range, and comprise nine categories, including cloth, different kinds of paint, human skin, leaves, metals, papers of different colours, plastic, porcelain and wood types. The canonical illuminant library is acquired with similar settings and consists of four light sources (tungsten, incandescent, fluorescent and sunlight). The spectra for the end members and canonical light sources are normalised so that the integrated reflectance across the visible range is unity. Our image data is given by 77 multispectral images representing three categories (landscapes, people and still life) acquired under a wide variety of lighting conditions spanning from outdoor settings to indoor locations. The imagery is composed of spectra sampled at intervals of  $10nm$  in the range between  $430nm$  and  $650nm$ , *i.e.* 23 bands.

To normalise the spectral images and the end-member spectra to the same spectral resolution, we employed the B-Spline representation in [14] to re-interpolate the end-member reflectance spectra and canonical light power spectra at 27, 36, 45, 54, 63 and 72 equally spaced wavelengths



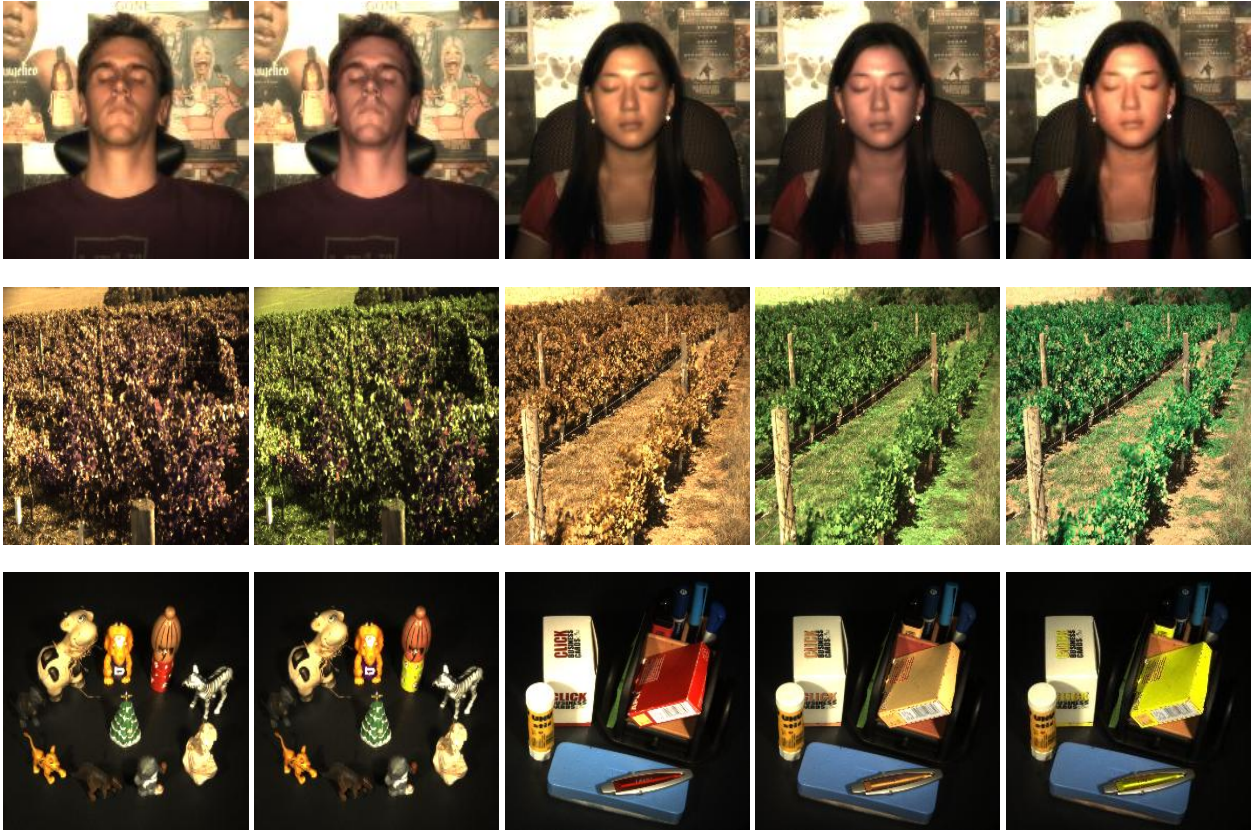


Figure 4. Sample results for the recovery of user profiles. Left-most column: Sample input images presented to the user; Second column: Images after user modifications have been made; Third column: Pseudocolour for novel imagery in the data set whose RGB is computed using colour matching functions; Fourth column: Pseudocolour images obtained using the user profiles computed from the edits provided by the users in the second column with  $\tau = 5$  in Equation 13; Fifth column: Pseudocolour images obtained using the user profiles with  $\tau = 0$ . Each row corresponds to a different user profile.

in the  $430 - 720nm$  region, yielding libraries of spectra sampled at between  $4nm$  and  $11nm$  steps. Next, we selected from these libraries a number of end-members equal to the number of sampling bands. From the 297 spectra in our initial library, we selected those that yield the lowest reconstruction error following a down-sampling operation on them so as to arrive at the same spectral resolution as the spectral images. For our imagery, we up-sampled the pixel spectra to achieve the spectral resolution corresponding to the end-member library size. Note that this is important since otherwise the problem of recovering the mixture coefficients may become an under-constrained one that has trivial or non-unique solutions for  $\rho_{m,v}$ .

We now turn our attention to the colour yielded by our method as compared with the direct application of the colour matching functions in [25]. To this end, we produced pseudocolour imagery from our multispectral images using Equation 2. We also recovered the RGB images using Equation 3. In our experiments, the minimisation of the cost function in Equation 10 took, on average, 4.7 seconds on

an Intel Corel 2 Duo 3.00GHz PC. The color mapping update step in Equation 13 was solved using a quasi-Newton method, taking an average of 5.6 iterations to converge in 0.6 seconds. The initial and terminal temperatures for the deterministic annealing were set to 0.02 and 0.00025, respectively.

In Figure 3 we show the mean-absolute error between the pseudocolour imagery computed using the colorimetric standard and that yielded by our approach when the predetermined colour mapping functions are used. In the figure, each trace represents a different size of the end-member library, where the x-axis indicates the number of end members used to recover the colour for each pixel spectra. It can be observed in the figure that the reconstruction error is small when predetermined colour mapping functions are used. The error is monotonically decreasing with respect to the number of end-member spectra used. As the end-member library increases in size, the reduction in error becomes less apparent. This suggests a trade-off between complexity and performance. As a result, in our system,

and for the final set of results shown here, we used the end-member library with 54 spectra and set the number of end members per object material to 4.

Finally, we illustrate the use of individual profiles to represent colour from multispectral imagery. To recover these profiles, we asked users to modify colours on 10 randomly selected images in our data set according to their material preferences. These profiles can then be used to generate the RGB images for the rest of our imagery. In left-most column of Figure 4, we show sample pseudocolour images presented to the user. In the figure, each row corresponds to a different user. The second column shows the images as modified by each user. In the third column, we show novel images rendered using the standard colour matching functions, and in the fourth and fifth columns, the ones corresponding to the user profiles with and without the use of aesthetics to moderate the rendering results, by setting  $\tau = 5$  and  $\tau = 0$  in Equation 13, respectively.

Note that no pair of profiles are exactly the same, with some users changing material colours to a great extent. For instance, the first user made subtle changes the skin hue, whereas the second user aggressively edited the green tones for chlorophyll. This, in turn, corrected the green hues for the vegetation in the other landscape imagery while preserving the brown tones on the fence poles. The third user changed the colour of the doll, which affected the cardboard box, the red letters on the white box and the red marker, all of which have turned yellow. This is since the end-member for a particular red dye in the library was modified on the corresponding profile. Also, note that the imagery in the fifth and fourth columns clearly reflects the effect of the aesthetic score in the recovered colour matching functions. This is particularly evident on the green hues for the landscape and the yellow on the still life scene.

## 6. Conclusions

In this paper, we have presented a method to produce color imagery from imaging spectroscopy data using color mappings computed from user input by imposing consistency across materials in the scene. Our consistency imposition approach is based upon a cost function which arises from the end-member affinity and the maximum entropy criterion. We have also described how user profiles can be recovered making use of a score based on a computational model of image aesthetics. The results on a data set of real world imagery and on the imagery obtained using sample user profiles show the effectiveness of our method.

## References

- [1] A. Levin, D. Lischinski, and Y. Weiss. Colorization using optimization. *ACM Transactions on Graphics*, 23(3):689–694, 2004.
- [2] E. Angelopoulou, R. Molana, and K. Daniilidis. Multispectral skin color modeling. In *Computer Vision and Pattern Recognition*, pages 635–642, 2001.
- [3] A. Barret and A. Cheney. Object-based image editing. *ACM Transactions on Graphics*, 21(3):777–784, 2002.
- [4] J. Bonnans, J. C. Gilbert, C. Lemaréchal, and C. Sagastizábal. *Numerical Optimization – Theoretical and Practical Aspects*. Universitext. Springer Verlag, Berlin, 2006.
- [5] D. H. Brainard. *Colorimetry*. McGraw-Hill, 1995.
- [6] CIE. *Commission Internationale de l’Eclairage Proceedings, 1931*. Cambridge University Press, 1932.
- [7] R. Clark, G. Swayze, K. Livo, R. Kokaly, S. Sutley, J. Dalton, R. McDougal, and C. Gent. Imaging spectroscopy: Earth and planetary remote sensing with the usgs tetracorder and expert system. *Journal of Geophysical Research*, 108(5):1–44, 2003.
- [8] R. Datta, D. Joshi, J. Li, and J. Z. Wang. Studying aesthetics in photographic images using a computational approach. In *European Conference on Computer Vision*, pages III:288–301, 2006.
- [9] M. S. Drew and G. D. Finlayson. Analytic solution for separating spectra into illumination and surface reflectance components. *Journal of the Optical Society of America A*, 24(2):294–303, 2007.
- [10] T. Ejaz, T. Horiuchi, G. Ohashi, and Y. Shimodaira. Development of a camera system for the acquisition of high-fidelity colors. *IEICE Transactions on Electronics*, E89–C(10):1441–1447, 2006.
- [11] G. D. Finlayson and M. S. Drew. The maximum ignorance assumption with positivity. In *Proceedings of the IS&T/SID 4th Color Imaging Conference*, pages 202–204, 1996.
- [12] G. R. Greenfield and D. H. House. Image recoloring induced by palette color associations. *Journal of WSCG*, 11:189–196, 2003.
- [13] B. K. P. Horn. Exact reproduction of colored images. *Computer Vision, Graphics, and Image Processing*, 26(135), 1981.
- [14] C. P. Huynh and A. Robles-Kelly. A nurbs-based spectral reflectance descriptor with applications in computer vision and pattern recognition. In *IEEE Conference on Computer Vision and Pattern Recognition*, 2008.
- [15] C. P. Huynh and A. Robles-Kelly. A solution of the dichromatic model for multispectral photometric invariance. *International Journal of Computer Vision*, 90(1):1–27, 2010.
- [16] E. T. Jaynes. Information Theory and Statistical Mechanics. *Phys. Rev.*, 106(4):620–630, 1957.
- [17] D. B. Judd, D. L. Macadam, G. Wyszecki, H. W. Budde, H. R. Condit, S. T. Henderson, and J. L. Simonds. Spectral distribution of typical daylight as a function of correlated color temperature. *Journal of the Optical Society of America*, 54(8):1031–1036, 1964.
- [18] D. S. Kirk, A. J. Sellen, C. Rother, and K. R. Wood. Understanding photowork. In *Proceeding of the SIGCHI conference on Human Factors in Computing Systems*, pages 761–770, 2006.
- [19] S. Kirkpatrick, C. D. Gelatt, and M. P. Vecchi. Optimization by simulated annealing. *Science*, 220(4598):671–680, 1983.
- [20] P. Longere and D. H. Brainard. Simulation of digital camera images from hyperspectral input. In C. van den Branden Lambrecht, editor, *Vision Models and Applications to Image and Video Processing*, pages 123–150. Kluwer, 2001.
- [21] Q. Luan, F. Wen, D. Cohen-Or, L. Liang, Y. Q. Xu, and H. Y. Shum. Natural image colorization. 2007.
- [22] J. Parkkinen, J. Hallikainen, and T. Jaaskelainen. Characteristic spectra of munsell colors. *Journal of the Optical Society of America A*, 6(2):318–322, 1989.
- [23] E. Reinhard, M. Adhikhmin, B. Gooch, and P. Shirley. Color transfer between images. *IEEE Computer Graphics and Applications*, 21(4):34–41, 2001.
- [24] S. A. Shafer. Using color to separate reflection components. *Color Research and Applications*, 10(4):210–218, 1985.
- [25] W. S. Stiles and J. M. Burch. N.P.L. colour-matching investigation: Final report 1958. *Optica Acta*, 6:1–26, 1959.
- [26] P. Vora, J. Farrell, J. Tietz, and D. Brainard. Image capture: Simulation of sensor responses from hyperspectral images. *IEEE Transactions on Image Processing*, 10(2):307–316, 2001.
- [27] B. A. Wandell. The synthesis and analysis of color images. *IEEE Transactions on Pattern Analysis and Machine Intelligence*, 9(1):2–13, 1987.
- [28] G. Wyszecki and W. Stiles. *Color Science: Concepts and Methods, Quantitative Data and Formulae*. Wiley, 2000.
- [29] K. Zuiderveld. *Contrast Limited Adaptive Histogram Equalization*, chapter Graphics Gems IV, pages 474–485. Academic Press, 1994.